Electronic Supplementary Material (ESI) for Materials Advances.

Supporting Information

Lanthanoid Coordination Compounds as Diverse Self-Templating Agents Towards Hierarchically Porous Fe–N–C Electrocatalysts

Itamar Salton,[a]= Karina Ioffe,[a]= Tomer Y. Burshtein,[a] Eliyahu M. Farber,[a] Nicola M. Seraphim,[a] Nofit Segal,[a] David Eisenberg*[a]

Synthetic procedures

Synthesis of lanthanoid iminodiacetates (Ln-IDA). $LnCl_3$ (Ln = La, Nd, Sm, Eu, Gd, Tb, Er, Yb) and IDA (molar ratio 1:3) were mixed in doubly deionized water (DDI) at 85 °C until a clear solution was obtained. The solution was then stirred and heated to 100 °C until most water evaporated. The remaining solutions then transferred to a vacuum oven to dry out at 40 °C for 48 hours. The precipitate was ground by mortar and pestle to a fine powder then washed with cold ethanol (96%). The resulting powder was vacuum dried again at 40 °C for 48 hours.

Synthesis of carbons. The Ln-IDA powders were pyrolyzed at 800 °C in Ar atmosphere for 2 h (heating to 360 °C at a rate of 2 °C/min, to 800 °C at a rate of 10 °C/min). These inorganic/carbon composites are denoted as LnX@NC, where Ln = La, Nd, Sm, Eu, Gd, Tb, Er, Yb, and X is the anion(s). The inorganic phase was dissolved in hydrochloric acid (1 M, 24 hours), and the resulting carbon was vacuum dried.

Iron transmetalation. To perform transmetalation of the nitrogen centers with iron, the procedures of Fellinger *et al.* were followed.[1–3] 20 mg of NC_{Ln} were dispersed in 25 mL methanol, followed by the addition of 25 mL of $FeCl_2·4H_2O$ solutions (≥ 99.0%, Sigma-Aldrich; 25 mM), and refluxing for 24 h. The samples obtained were washed in 0.5 M H_2SO_4 overnight to remove physisorbed metal ions, followed by thorough aqueous washing.

Material characterizations

Powder X-ray diffraction (PXRD) was recorded on a Rigaku Miniflex II instrument operating at 30 kV and 15 mA, at a wavelength of 1.54 Å. High resolution scanning electron microscopy (HRSEM) was done on a Zeiss-ultra+ at 4 kV and in-lens detector. N_2 adsorption–desorption isotherms were measured on a Micromeritics 3Flex instrument at 77 K, using vacuum-dried samples. The isotherms were analyzed using the two-parameter Brunauer–Emmett–Teller (BET) model for specific surface area (SSA, at P/P^0 values of 0.01–0.15) and by density functional theory (DFT) isotherm fitting for pore size distribution (using the adsorption branch of the isotherm). Raman spectroscopy was performed on a Horiba LabRam HR Evolution Raman microscope using ×10 lens, 532 nm laser excitation wavelength, and 1800 grating. First-order Raman spectra were fitted iteratively with four Lorentzian components. The degree of graphitization is correlated to the intensity ratio between the D and G Raman peaks (I_D/I_G), from which the characteristic length of graphitic domains in the *a* direction (L_a) was calculated.[4] X-ray photoelectron spectroscopy (XPS) was collected on a PHI VersaProbe III scanning microprobe supplied from Physical Instruments at UHV $\sim 10^{-10}$ Torr, step size 0.05 eV. Peaks were calibrated using the C 1s position (284.8 eV), and deconvoluted in CasaXPS software. Elemental analysis by inductively coupled plasma mass spectroscopy (ICP-MS) was performed by Mikroanalytisches Labor Kolbe. Thermogravimetric analysis with differential scanning calorimetry (TGA-DSC) was performed under Ar flow (10 mL/min), heating to 200 °C at a rate of 10 °C/min, then to 300 °C at 1 °C/min, then to 1000 °C at 10 °C/min, and then cooling to room temperature at a rate of 50 °C/min. Microscopes: high-resolution scanning electron microscopy (Zeiss-ultra+, 3 kV) and high-resolution transmission electron microscopy (FEI Tecnai and FEI Titan Themis, 200 kV).

Electrochemical experiments

Inks of the catalytic powders were prepared according to the following proportions: 0.40 mL of isopropanol, 10 µL of Nafion (5 wt % in water/isopropanol), and 2.5 mg of NC_{Ln} powder, when were sonicated and stirred. A 20 µL drop of inks was applied to the glassy carbon working electrode (ϕ = 5 mm, A = 0.196 cm^2) and and dried at 50 °C in air. Electrochemical experiments were performed with a bipotentiostat (BioLogic 600) using a three-electrode glass cell, filled with KOH (1 M, 100 mL), and stabilized at 25.0 ± 0.1 °C. A saturated calomel electrode (SCE) was used as a reference electrode, and a graphite rod was used as a counter electrode. Potentials were reported vs reversible hydrogen electrode (RHE) by adding 1.07 for pH 14. Nitrogen (99.999%) were bubbled for 30 min to saturate the solution and were flowed above the solution during the experiments. The electrocatalytic HzOR activity of the electrocatalysts was evaluated in the potential range –0.9 V to 0.4 V vs. SCE. in 1 M KOH containing 10, 60 and 100 mM N_2H_4. The identity of hydrazine as the oxidized species is further corroborated by the linear dependence of peak current density on hydrazine concentration.

Nitrite poisoning experiments, based on Malko *et al.*[5] proceeded as follows:

1. HzOR before poisoning: Washing the catalyst-covered RDE in DI. Cyclic voltammetry in N_2-saturated 1 M NaOH (10 mV/s, –0.9 to +0.1 V vs SCE), before and after adding 100 mM N_2H_4.
2. Poisoning: Immersion of the electrode in a 0.125 M $NaNO_2$ solution at open circuit potential (OCP) for 5 minutes, rotating at 300 rpm.
3. Nitrite to nitrosyl reaction: Immersion of the electrode into 0.5 M H_2SO_4 at OCP for 1 minute, rotating at 300 rpm. Washing the electrode in DI.
4. HzOR after poisoning: Cyclic voltammetry in N_2-saturated 1 M NaOH with 100 mM N_2H_4 (10 mV/s, –0.9 to +0.1 V vs SCE).
5. Reductive desorption of poison: Cyclic voltammetry in N_2-saturated 0.5 M H_2SO_4 (10 mV/s, +0.6 to –0.7 V vs SCE).
6. HzOR after full recovery: Cyclic voltammetry in N_2-saturated 1 M NaOH with 100 mM N_2H_4 (10 mV/s, –0.9 to +0.1 V vs SCE). Washing the electrode in DI.

Cyanide poisoning proceeded according to a similar method.[6] The inhibitor (CN^-) was added as NaCN (97 %, Alfa Aesar) to the electrolyte in a concentration of 0.04 M, without the need for step 3 above.

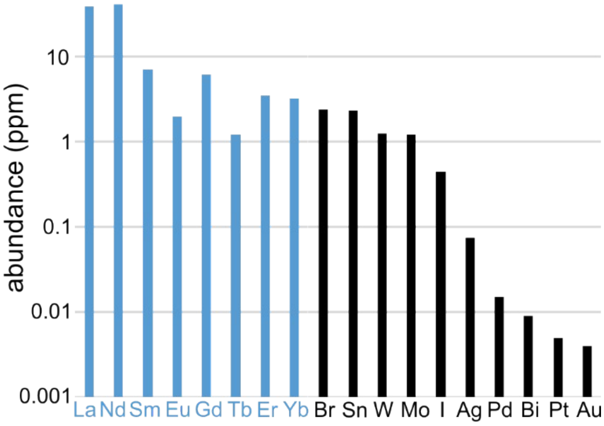

Figure S1. Abundance of elements in the earth's crust.[7]

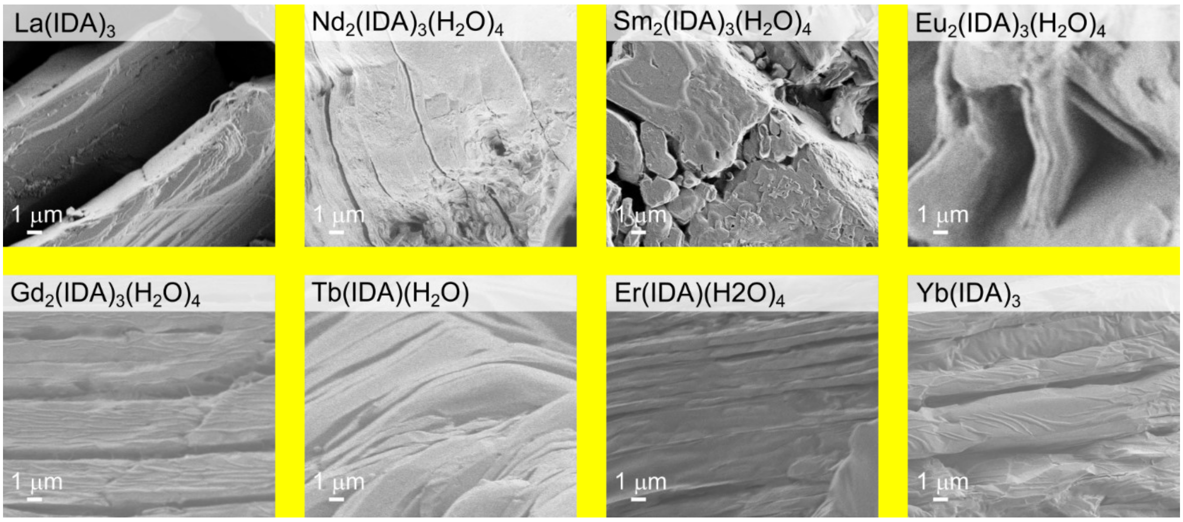

Figure S2: SEM micrographs of the Ln-IDA powders.

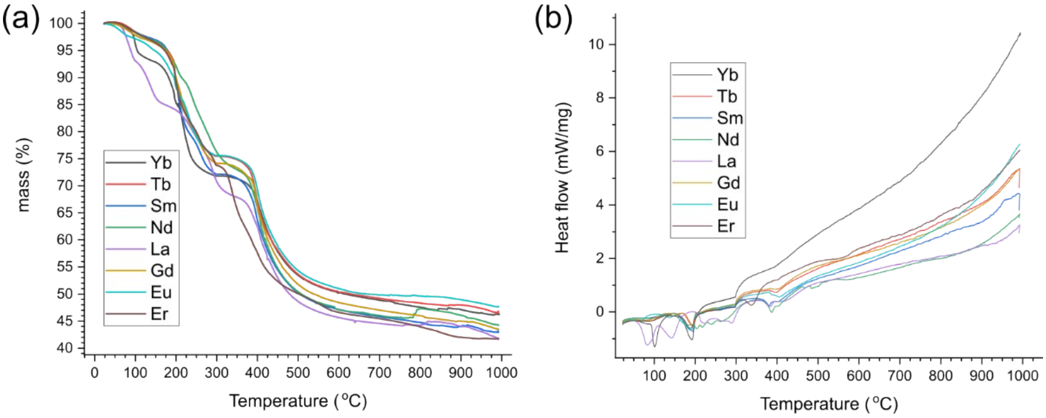

Figure S3: (a) Thermal gravimetric analysis, (b) differential scanning calorimetry, in argon, of the eight lanthanoid iminodiacetate precursors.

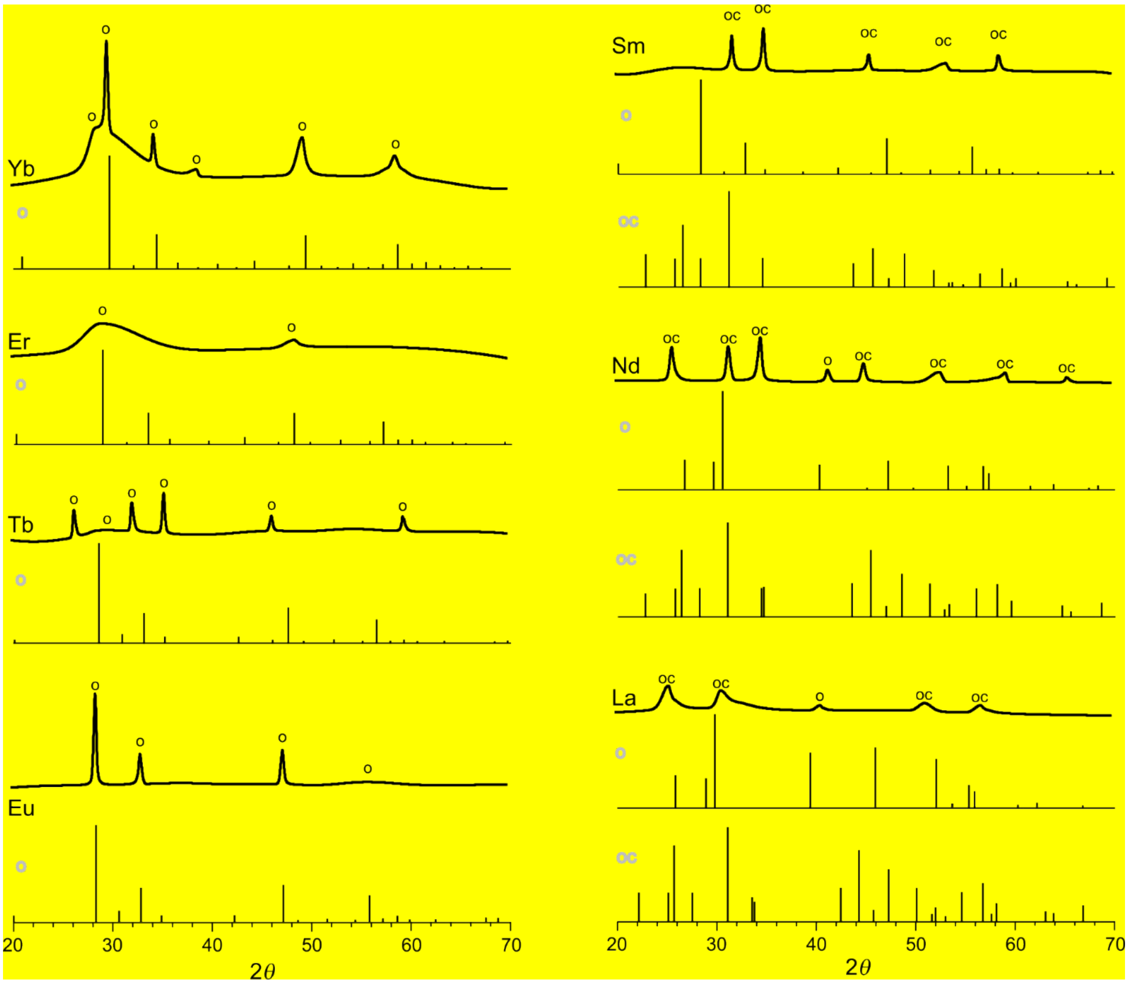

Figure S4: X-ray diffractograms with visual assignments. Ln_2O_3 oxides are marked o (JCPDS: La 05-0602, Nd 43-1023, Eu 83-7117, Tb 76-0156, Er 08-8239, Yb 41-1106) and $Ln_2O_2CO_3$ oxycarbonates are marked oc (JCPDS: La 37-0804, Nd 37-0806, Sm 37-0807).

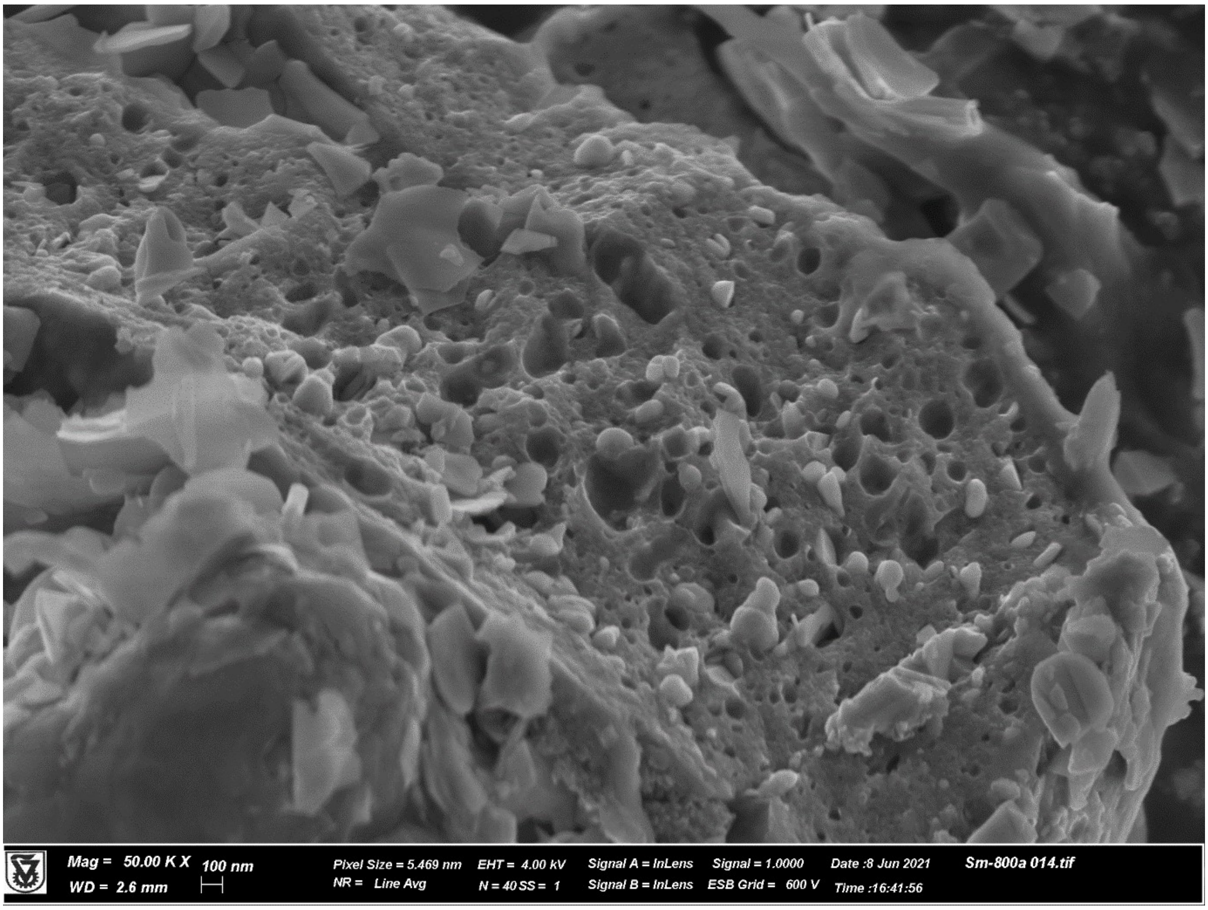

Figure S5: SEM micrograph of SmX@NC.

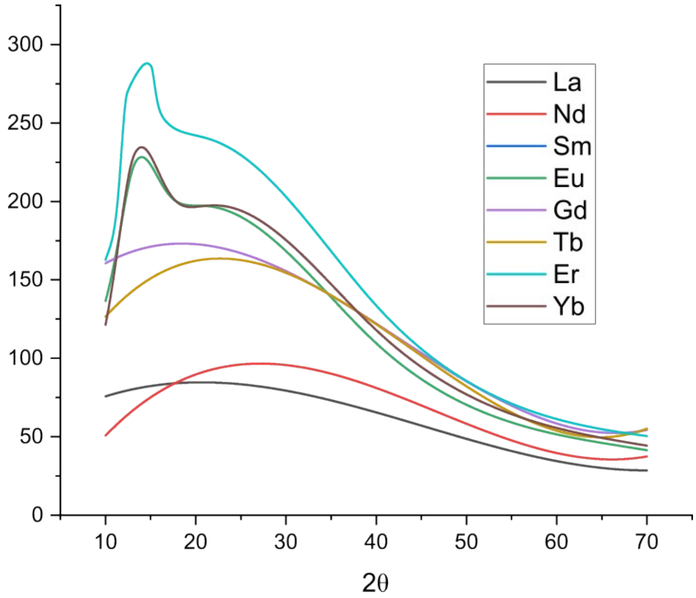

Figure S6. XRD of the eight NC$_{Ln}$ carbons after the acid wash, showing no trace of the oxides or oxycarbonates.

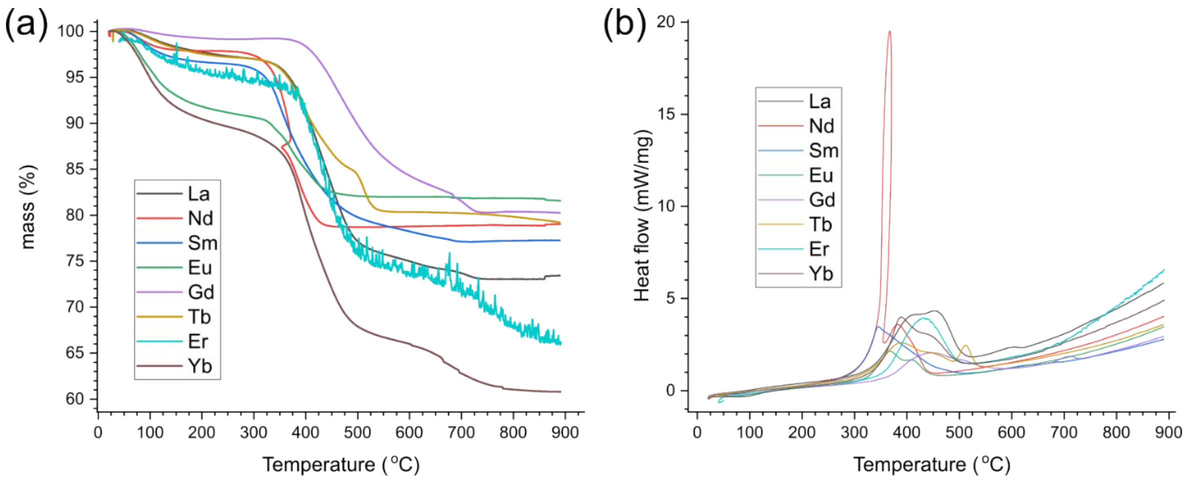

Figure S7: (a) Thermal gravimetric analysis, (b) differential scanning calorimetry, in air, of the eight LnX@NC materials. The first mass loss around ~200 °C corresponds to dehydration, and the second around ~400 °C corresponds to complete oxidation of any remaining metal ions to the oxide. The final gradual heat release > 600 °C is due to burn-off of the carbon.

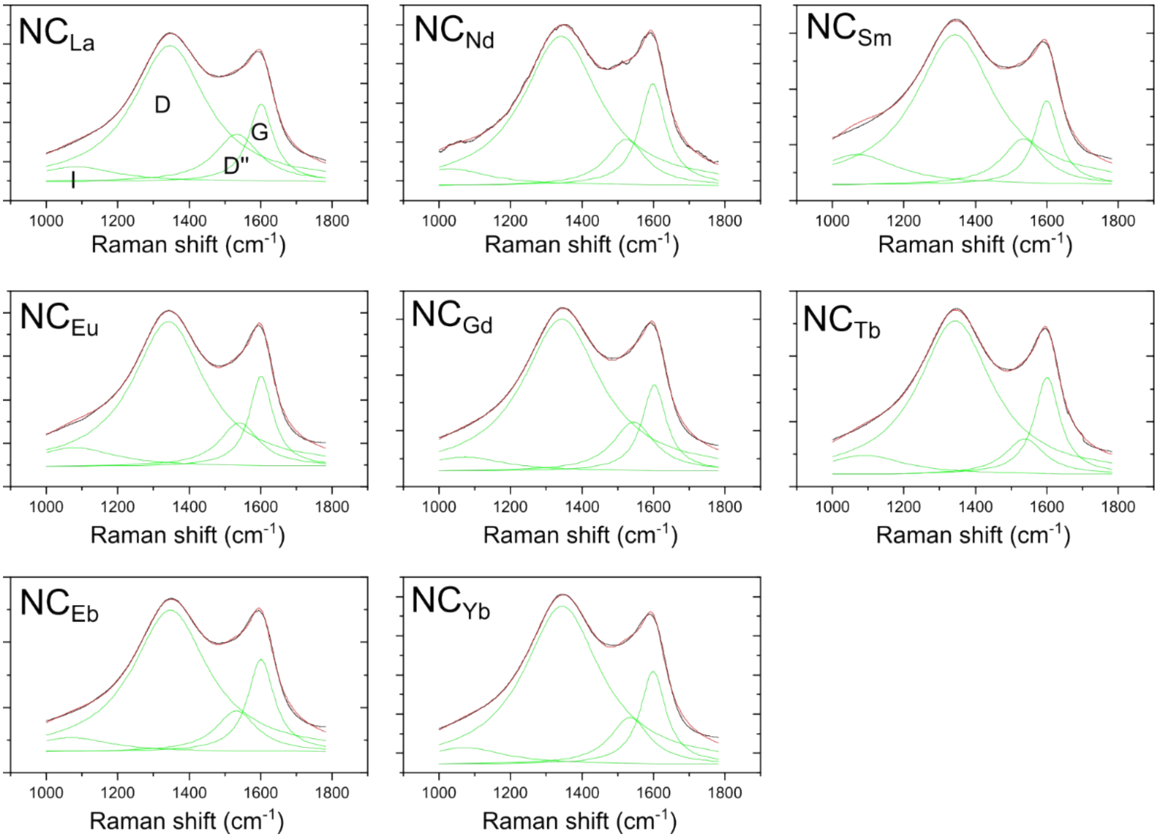

Figure S8: Raman spectra of the eight NC$_{Ln}$ materials, deconvoluted into 4 bands as shown for NC$_{La}$.

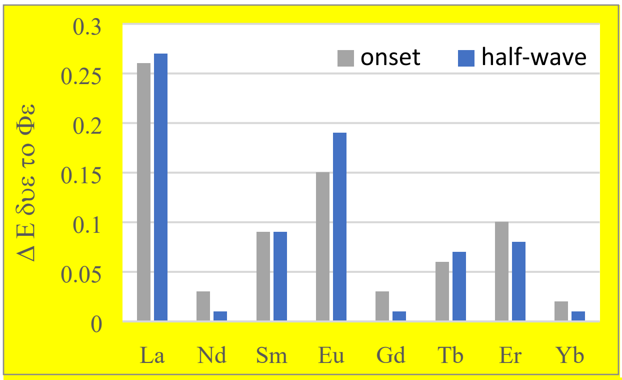

Figure S9: Onset and half-wave potentials (V vs. RHE), before and after iron transmetalation.

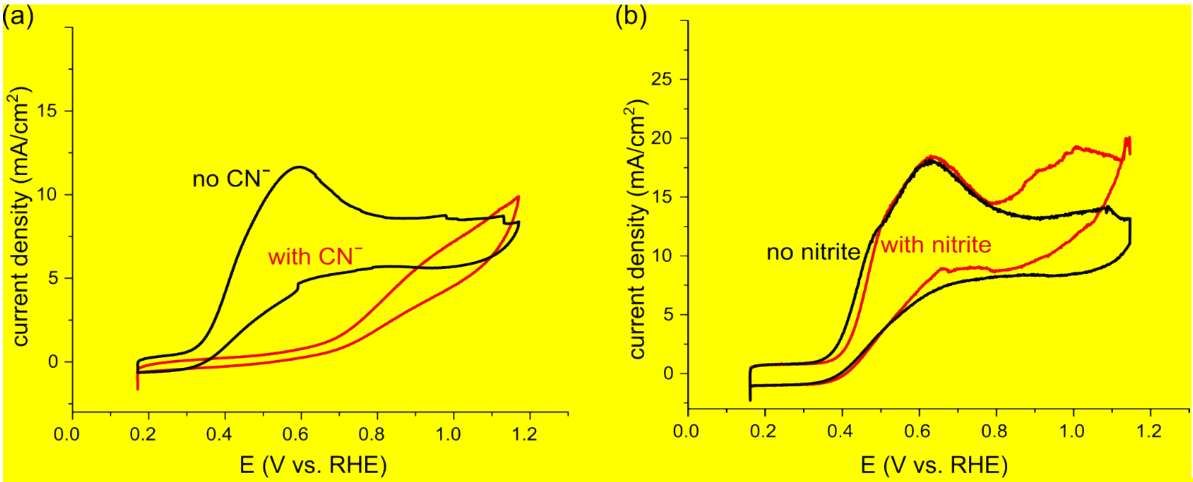

Figure S10: Poisoning experiments by (a) cyanide, and (b) nitrite ions. See Supporting Information for experimental procedure and conditions.

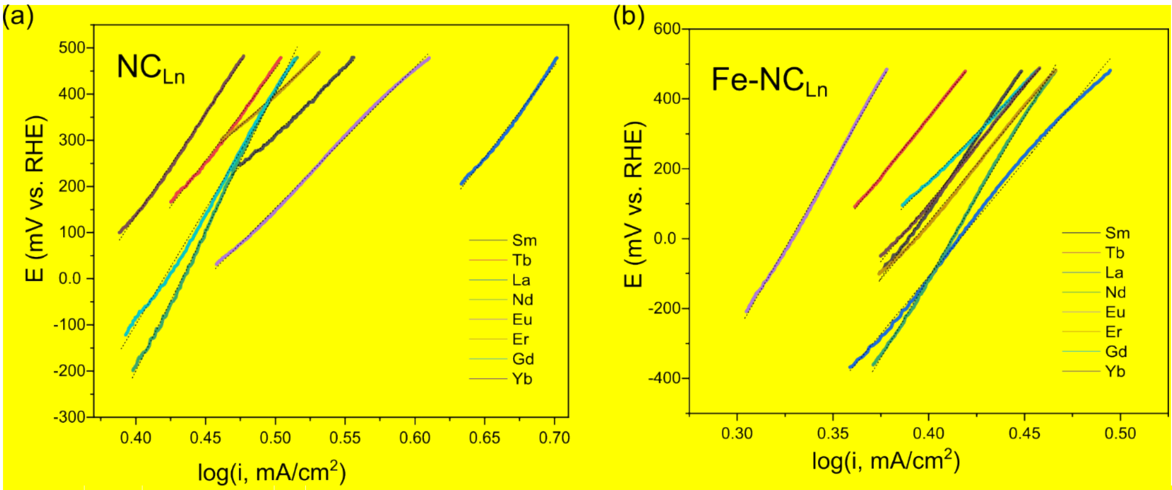

Figure S11: Tafel plots of the iron-free (NC$_{Ln}$) and iron-imprinted (Fe-NC$_{Ln}$) electrocatalysts. See Table S4 for slopes.

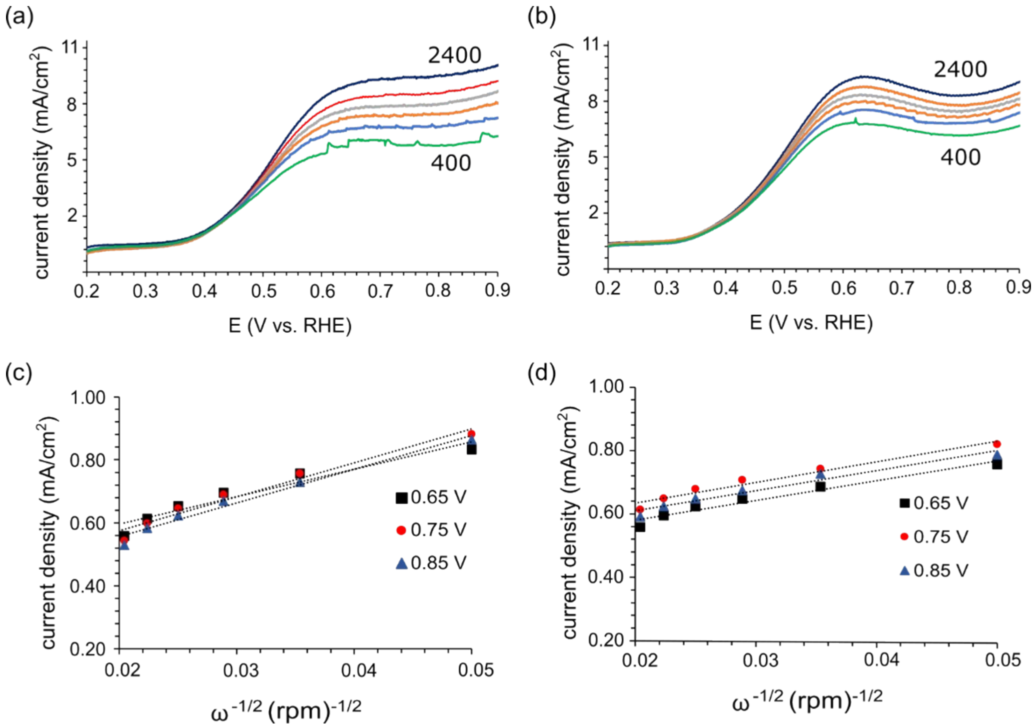

Figure S12: Rotating disk electrode studies of two HzOR electrocatalysis, NC_{Yb} (a,c) and NC_{Eu} (b,d) in 1.0 M KOH. (a,c) LSVs at different rotation speeds in rpm, 10 mV s^{-1}. (c,d) Koutecký-Levich analysis.

Table S1. Distribution of nitrogen moieties, from deconvoluted XPS N 1s spectra (at%).

	Fe-NC$_{Eu}$	**Fe-NC$_{Sm}$**
pyridinic (N_p)	25.8	24.3
metallic (N_{Me})	32.8	24.9
pyrrolic (N_{py})	15.0	17.5
quaternary (N_q)	15.0	17.5
graphitic (N_{gr})	5.4	6.4
N oxide (N_{ox})	6.0	9.4

Table S2. Onset and half-wave potentials (V vs. RHE), before and after iron transmetalation.

	NC		Fe-NC		Δ due to Fe (mV)	
	E_{onset}	$E_{½}$	E_{onset}	$E_{½}$	ΔE_{onset}	$\Delta E_{½}$
La	0.61	0.76	0.35	0.49	**260**	**270**
Nd	0.38	0.50	0.35	0.49	**30**	**10**
Sm	0.44	0.59	0.35	0.50	**90**	**90**
Eu	0.44	0.58	0.29	0.39	**150**	**190**
Gd	0.39	0.52	0.36	0.51	**30**	**10**
Tb	0.39	0.53	0.33	0.46	**60**	**70**
Er	0.45	0.57	0.35	0.49	**100**	**80**
Yb	0.36	0.50	0.34	0.51	**20**	**10**

Table S3. State-of-the-art Fe-based, PGM-free HzOR electrocatalysts, arranged by E_{onset} (1 M KOH).

Catalyst	**E_{onset} vs. RHE**	**Year**	**Ref.**
Fe-N_x@NC	0.25	2020	[8]
Fe-N_x@NC	0.25	2020	[9]
Fe-N_x@NC	**0.32**	**2022**	**this work**
Fe-N_x@CNT	0.32	2021	[10]
Fe_3C / Fe-N_x@NC	0.34	2019	[11]
Fe-N_x@NC	0.34	2021	[12]
Fe-N_x@NC	0.35	2021	[13]
Fe-N_4 corrole @ C	0.39	2022	[14]

Table S4. Tafel slopes of iron-free (NC_{Ln}) and iron-imprinted (Fe-NC_{Ln}) electrocatalysts (Figure S11).

	Tafel slope (mV/dec)	
Ln:	**NC_{Ln}**	**Fe-NC_{Ln}**
La	251	152
Nd	165	109
Sm	351	124
Eu	327	104
Gd	199	180
Tb	251	147
Er	367	152
Yb	225	149
average	**270**	**140**
st. dev.	**70**	**25**

References

1 A. Mehmood, J. Pampel, G. Ali, H. Y. Ha, F. Ruiz-Zepeda and T.-P. Fellinger, *Adv. Energy Mater.*, 2018, **8**, 1701771.

2 D. Menga, F. Ruiz-Zepeda, L. Moriau, M. Šala, F. Wagner, B. Koyutürk, M. Bele, U. Petek, N. Hodnik, M. Gaberšček and T.-P. Fellinger, *Adv. Energy Mater.*, 2019, **9**, 1902412.

3 D. Menga, J. L. Low, Y.-S. Li, I. Arčon, B. Koyutürk, F. Wagner, F. Ruiz-Zepeda, M. Gaberšček, B. Paulus and T.-P. Fellinger, *J. Am. Chem. Soc.*, 2021, **143**, 18010–18019.

4 L. G. Cançado, K. Takai, T. Enoki, M. Endo, Y. A. Kim, H. Mizusaki, A. Jorio, L. N. Coelho, R. Magalhães-Paniago and M. A. Pimenta, *Appl. Phys. Lett.*, 2006, **88**, 163106.

5 D. Malko, A. Kucernak and T. Lopes, *J. Am. Chem. Soc.*, 2016, **138**, 16056–16068.

6 F. J. Pérez-Alonso, C. Domínguez, S. A. Al-Thabaiti, A. O. Al-Youbi, M. Abdel Salam, A. A. Alshehri, M. Retuerto, M. A. Peña and S. Rojas, *J. Power Sources*, 2016, **327**, 204–211.

7 W. M. Haynes, in *CRC Handbook of Chemistry and Physics, 95th Edition*, CRC Press, Hoboken, 95th edn., 2014, pp. 14–19.

8 Y.-C. Wang, L.-Y. Wan, P.-X. Cui, L. Tong, Y.-Q. Ke, T. Sheng, M. Zhang, S.-H. Sun, H.-W. Liang, Y.-S. Wang, K. Zaghib, H. Wang, Z.-Y. Zhou and J. Yuan, *Small*, 2020, **16**, 2002203.

9 Y. Zheng, F. He, M. Chen, J. Zhang, G. Hu, D. Ma, J. Guo, H. Fan, W. Li and X. Hu, *ACS Appl. Mater. Interfaces*, 2020, **12**, 38183–38191.

10 J. Zhang, Y. Wang, C. Yang, S. Chen, Z. Li, Y. Cheng, H. Wang, Y. Xiang, S. Lu and S. Wang, *Nano Res.*, 2021, **14**, 4650–4657.

11 T. Y. Burshtein, E. M. Farber, K. Ojha and D. Eisenberg, *J. Mater. Chem. A*, 2019, **7**, 23854–23861.

12 T. Y. Burshtein, I. Agami, M. Sananis, C. E. Diesendruck and D. Eisenberg, *Small*, 2021, 2100712.

13 T. Y. Burshtein, D. Aias, J. Wang, M. Sananis, E. M. Farber, O. M. Gazit, I. Grinberg and D. Eisenberg, *Phys. Chem. Chem. Phys.*, 2021, **23**, 26674–26679.

14 Y. Shahaf, A. Mahammed, A. Raslin, A. Kumar, E. M. Farber, Z. Gross and D. Eisenberg, *ChemElectroChem*, 2022, **9**, e202200045.